http://www.jstage.jst.go.jp/browse/biophysics

BIOPHYSICS

Vol. 6, pp. 27–36 (2010)
doi: 10.2142/biophysics.6.27

Molecular modeling of the HAMP domain of sensory rhodopsin II transducer from *Natronomonas pharaonis*

Koro Nishikata[1], Sotaro Fuchigami[1], Mitsunori Ikeguchi[1] and Akinori Kidera[1,2]

[1]*Graduate School of Nanobioscience, Yokohama City University, Yokohama 230-0045, Japan*
[2]*Research Program for Computational Science, RIKEN, Wako 351-0198, Japan*

Received 1 February, 2010; accepted 16 February, 2010

The halobacterial transducer of sensory rhodopsin II (HtrII) is a photosignal transducer associated with phototaxis in extreme halophiles. The HAMP domain, a linker domain in HtrII, is considered to play an important role in transferring the signal from the membrane to the cytoplasmic region, although its structure in the complex remains undetermined. To establish the structural basis for understanding the mechanism of signal transduction, we present an atomic model of the structure of the N-terminal HAMP domain from *Natronomonas pharaonis* (HtrII: 84–136), based on molecular dynamics (MD) simulations. The model was built by homology modeling using the NMR structure of Af1503 from *Archaeoglobus fulgidus* as a template. The HAMP domains of Af1503 and HtrII were stable during MD simulations over 100 ns. Quantitative analyses of inter-helical packing indicated that the Af1503 HAMP domain stably maintained unusual knobs-to-knobs packing, as observed in the NMR structure, while the bulky side-chains of HtrII shifted the packing state to canonical knobs-into-holes. The role of the connector loop in maintaining structural stability was also discussed using MD simulations of loop deletion mutants.

Key words: Molecular dynamics simulation, Coiled-coil, Signal transduction, Homology model, Af1503

The halobacterial transducer of sensory rhodopsin II (HtrII) from *Natronomonas pharaonis* transfers the repellent signal against blue-green light from sensory rhodopsin II to cytoplasmic receptor proteins, eventually leading to negative phototaxis[1–4]. The HAMP domain of HtrII, located between the transmembrane and the cytoplasmic regions, is believed to play a key role in transmitting the photosignal[5–9].

The crystal structure of sensory rhodopsin II/HtrII complex has been solved for the ground state[10] as well as for the K and the M states[11]. These models did not resolve the coordinates of the HAMP domain (residues 84–136). On the other hand, the structural basis of the HAMP domain was established by NMR analysis of the HAMP domain of a hypothetical protein Af1503 from *Archaeoglobus fulgidus*, a homodimeric four-helix parallel coiled-coil[12]. It has also been suggested that the HAMP domains of the chemotaxis receptor Tsr[13,14], the aerotaxis receptor Aer[15] and the phototaxis transducer HtrII[16] have four-helix parallel coiled-coils similar to the NMR structure.

Based on the structural information of the HAMP domain, we built a model structure of the N-terminal HAMP domain of *Natronomonas pharaonis* HtrII using homology modeling on the basis of the NMR structure of Af1503[12], followed by structure refinement using extended molecular dynamics (MD) simulations. Although the sequence identity between the HAMP domain of HtrII and the corresponding portion of Af1503 is only 25%, the presence of coiled-coils in both structures allows us to perform a reliable sequence alignment and homology modeling.

Extended MD simulations (more than 100 ns) can be a stringent test of the stability of protein models. We performed MD simulations of the HAMP domains of Af1503 and HtrII in explicit water for 100 and 200 ns, respectively, to confirm their stability. Based on the results of the MD

Corresponding author: Akinori Kidera, Graduate School of Nanobioscience, Yokohama City University, Yokohama 230-0045, Japan.
e-mail: kidera@tsurumi.yokohama-cu.ac.jp

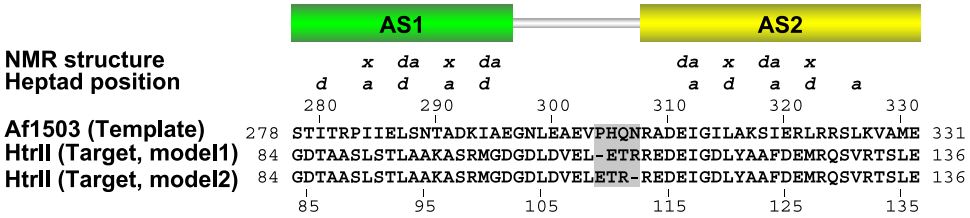

Figure 1 Sequence alignment between the HAMP domains of Af1503 and HtrII. Two different alignments (model 1 and model 2) were constructed. The gray shaded region delineates the difference between the two alignments. AS1 and AS2 denote the helices observed in the NMR structure. The positions noted by *x* and *da*, and *a* and *d*, are according to references 5 and 12, respectively.

simulations, we examined the structural differences between the HAMP domains of Af1503 and HtrII associated with the coiled-coil structure and the role of the connector loop in the structural stability.

Hulko *et al.* suggested that the inter-helix packing observed in the NMR structure of the HAMP domain is unusual *x-da* form (*knobs-to-knobs* packing) which is related to the canonical *a-d* form of coiled-coil (*knobs-into-holes*) by a 26° (~180°/7 related to the heptad repeat) rotation of each helix[12]. Based on this observation, they proposed a mechanism for the signal transduction in which the HAMP domain interconverts the inter-helix packing between knobs-to-knobs and knobs-into-holes. We determined the packing state on a quantitative basis using the *side-chain crick angle*, an extension of the *crick angle* defined by Strelkov and Burkhard's TWISTER program[17]. We found that the packing of the Af1503 HAMP domain was stably maintained in the knobs-to-knobs state for 100 ns, and that no indication of the transition to the knobs-into-holes state. On the other hand, we observed that HtrII assumed the knobs-into-holes form.

We also investigated that the role of the connector loops in the stability of the HAMP domain. Using MD simulations of loop deletion mutants of the HAMP domain, we found that both HAMP domains were stable even without the connector loop. This indicates that inter-helix packing is the main source of the HAMP domain stability, even though many interactions were found between the helices and the loops.

Methods

Homology modeling of the HAMP domain

A model of the N-terminal HAMP domain of *Natronomonas pharaonis* HtrII (residues 84–136) was built using homology modeling based on the NMR structure of *Archaeoglobus fulgidus* Af1503 (residues 278–331; PDBid: 2asw)[12]. We evaluated two different sequence alignments; one obtained by a Needleman and Wunsch type algorithm[18] with BLOSUM62[19] (Fig. 1, model 1), and the other obtained with PAM70[20] (model 2). Both alignments were obtained with gap opening (=11) and extension (=1) penalties. The alignments differ only in three residues and a gap, but this resulted in a large change in the stability of the connector loop (described below). The common part of the two alignments was confirmed by the *x-da* pattern in the NMR structure[12], and the heptad sequence repeats of the helices predicted for the secondary structures[5]. The coordinates of the homology model were generated using MODELLER (version 8.2)[21], followed by refinement of the side-chain conformations using SCWRL (version 3.0)[22]. The N-terminal and C-terminal residues were acetylated and amidated, respectively, to avoid the influence of charges. The model was validated by WHAT_CHECK[23] and PROCHECK[24]. The HAMP domain model was then relaxed in an explicit water environment by molecular dynamics simulations, using the MD program MARBLE[25] according to the protocol described below. The model was solvated in a periodic boundary box of water[26] and subject to energy minimization, followed by equilibration. Product runs were then performed without restraints. The simulation system for HtrII consists of a box of 64 Å×55 Å×44 Å containing 4,300 water molecules and 14 Na^+ ions (14,600 atoms in total). The reference system for Af1503 was contained in a box of 66 Å×50 Å×45 Å with 4,200 water molecules and 2 Na^+ ions (14,200 atoms in total).

Modeling of the loop deletion model

The loop deletion mutants of the HtrII and Af1503 HAMP domains were modeled by removing the connector loops (HtrII: 103–114; Af1503: 297–309). The C-terminals of the AS1 helix were amidated and the N-terminals of the AS2 helix were acetylated (see Fig. 1 for the assignment). The loop deletion mutant of Af1503 was contained in a box of 66 Å×47 Å×49 Å with 4,500 water (14,800 atoms in total), while the HtrII deletion mutant was in a box of 64 Å×48 Å×50 Å with 4,500 water and 8 Na^+ ions (14,700 atoms in total).

Molecular dynamics simulations

All MD simulations were carried out using the program MARBLE[25], with the force field parameters of CHARMM22[27] corrected by CMAP[28] for proteins, and TIP3P[29] for water. Electrostatic energy was calculated without a cutoff operation using the particle mesh Ewald method with periodic boundary conditions[26]. The Lennard-Jones interactions were

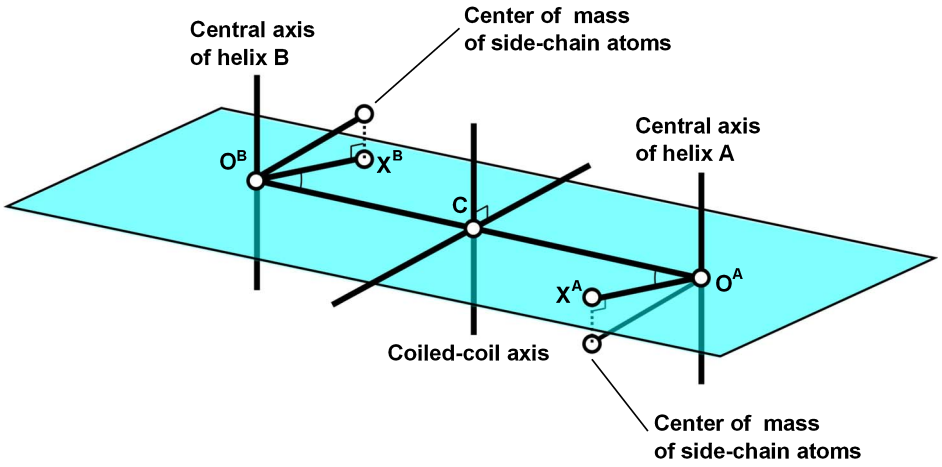

$$Side-chain\ crick\ angle = \frac{\angle \mathrm{CO^A X^A} + \angle \mathrm{CO^B X^B}}{2}$$

Figure 2 Schematic representation of the definition of the side-chain crick angle.

smoothly switched to zero over the range of 8–10 Å. The symplectic integrator for rigid bodies was used, treating CH_x, NH_x, SH, OH groups and water molecules as rigid bodies[25]. A time step of 2 fs was employed for the simulation. After energy minimization for 5,000 steepest descent steps, the system of the Af1503 HAMP domain was equilibrated for 200 ps in NPT ensemble (300.15 K and 1 atm), constraining the protein coordinates with a harmonic force constant of 1 kcal/mol/Å^2. The constraint was then gradually decreased to zero over 200 ps, and a product run of 100 ns was performed under NPT ensemble without constraint. The HtrII HAMP domain required 800 ps for equilibration, but the rest of the protocols were the same as those for Af1503. Finally, a product run was performed for 200 ns. To confirm the stability of polar interactions between connector loops and helical regions, we performed additional 100 ns simulations for the Af1503 and HtrII loop deletion mutants. Molecular graphics images were generated using PyMOL (Version 1.1r1).

Definition of the side-chain crick angle

To quantify coiled-coil packing and distinguish between knobs-into-holes and knobs-to-knobs, we calculated coiled-coil parameters using TWISTER[17]. To examine the direction of the side-chains in the core regions forming layers 1 to 4, we defined the *side-chain crick angle* in the following manner.

The crick angle is defined in TWISTER for two helices (A and B) in a coiled-coil by the average of the angles CO^AX^A and CO^BX^B, where O^A is a point on the central axis of helix A, C is the center of the coiled-coil defined by $(O^A+O^B)/2$, and X^A represents the position of C_α in helix A at which the crick angle is defined (Fig. 2). However, the original definition, based on the position of C_α, is not necessarily appropriate for rigorously defining the direction of a side-chain forming core packing in coiled-coil. To solve this problem, we defined the *side-chain crick angle* by changing the definition of X^A to the center of mass of nonhydrogen atoms in the side-chain projected onto the plane defined by O^AO^B and an axis perpendicular to the coiled-coil axis.

Results and discussion

The homology model of the HtrII HAMP domain

In spite of the apparent low sequence identity between the HAMP domains of Af1503 and HtrII (25%), there is only a limited possibility in the alignments. This limitation is originated from the strong pattern of the heptad repeat of the helix region and high sequence similarity in the loop region (78% similarity) besides the small region in the loop marked by the shade in Fig. 1 (residues 304–307 in Af1503 and 110–112 in HtrII). Accordingly, we have constructed two homology models of the HtrII HAMP domain, model 1 and model 2, which differ with respect to the shaded region in Fig. 1. A gap in HtrII is aligned to P304 in model 1 and N307 in model 2. Since the ϕ and ψ angles of P304 are –67.3° and 155.5°, respectively, E110 can be aligned to P304 with an ordinary torsional energy in model 2. During MD simulations of model 1, we found that a connector loop became unstable and produced a root-mean-square fluctuation (RMSF) for C_α atoms exceeding 2 Å within 100 ns (Supplementary Fig. S1), while model 2 maintained a stable structure of the loop region with small RMSF values (discussed in further detail below). Therefore, we adopted model 2 in the following discussion.

Stability of the HAMP domains

The root-mean-square-displacements (RMSD) of the

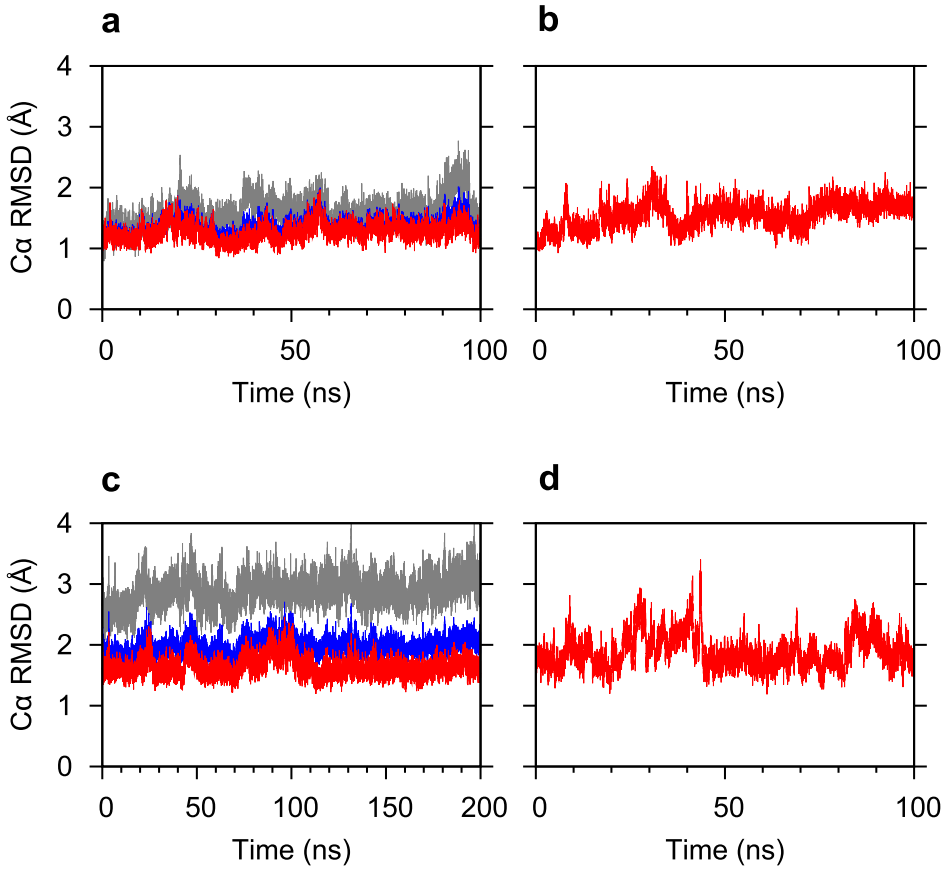

Figure 3 Time evolution of the root mean square displacement (RMSD=$\langle(\mathbf{r}_i - \mathbf{R}_i)^2\rangle^{1/2}$ where $\mathbf{r}_i$ is the coordinates of atom i of the target structure superimposed upon the reference structure $\mathbf{R}_i$, and $\langle\ \rangle$ denotes the average) for C_α atoms of the Af1503 HAMP domains from the NMR structure (PDBid: 2asw) during the simulation. The RMSD values were obtained by superimposition of the helix regions, AS1 and AS2 (Af1503: 278–296 and 310–331; HtrII: 84–102 and 115–136). The values presented here is the average for the two chains. (a) Af1503, (b) the Af1503 loop deletion mutant, (c) HtrII, and (d) the HtrII loop deletion mutant. Blue: RMSD for the entire HAMP domain; Red: RMSD for the helices only; Gray: RMSD for the connector loops only (Af1503: 297–309; HtrII: 103–114).

HAMP domain from the NMR structure (PDBid: 2asw) are plotted against the simulation time in Figs. 3a and 3c. The Af1503 HAMP domain was stable over a period of 100 ns, maintaining the original NMR structure even in the loop region. The RMSD value for the helices and the loop region averaged over the last 50 ns were 1.32 Å, and 1.67 Å, respectively. The HtrII HAMP domain was also stable in the helical regions (RMSD=1.61 Å), but in the loop region the structure appeared to change considerably compared to the template structure based on the NMR structure (RMSD= 2.96 Å). As discussed in more detail below, the large RMSD value for the HtrII HAMP domain was caused by the process of optimizing the template structure rather than flexibility of the loop region.

Structural stability is represented better by the RMSF values than the RMSD data. Figure 4a shows the RMSF values for C_α atoms of the Af1503 HAMP domain calculated for the last 50 ns of the trajectory. The stability of the Af1503 HAMP domain was confirmed by the small RMSF values, except for the flexible terminal residues. There are two minima in the RMSF values for the connector loop region, corresponding to L299 and V303. These two residues are stabilized during the simulation by hydrophobic contacts, L299-L326 and V303-I319/E320 (Fig. 5a). Hulko *et al.* pointed out that these residues are conserved during evolution and their contacts contribute to the stability of the connector loop[12].

The HtrII HAMP domain (Fig. 4c) is also stable; its RMSF values are only slightly larger than those for the Af1503 HAMP domain, but remain at a low level both in the helix and loop regions. Two residues showing small RMSF values, L105 and L109 (corresponding to Af1503 residues L299 and V303, respectively), are also stabilized by hydrophobic contacts, L105-V131 and L109-F124/D125 (Fig. 5c). The contact partners V131 and F124/D125 are also correctly aligned to the Af1503 counterparts L326 and I319/E320, respectively. Using mutational analyses of *E. coli* Tsr, Ames *et al*. showed that L237 and I241 (corresponding to L299 and V303 in Af1503, respectively) are involved in the packing interaction with AS2 helices[30]. This suggests that these

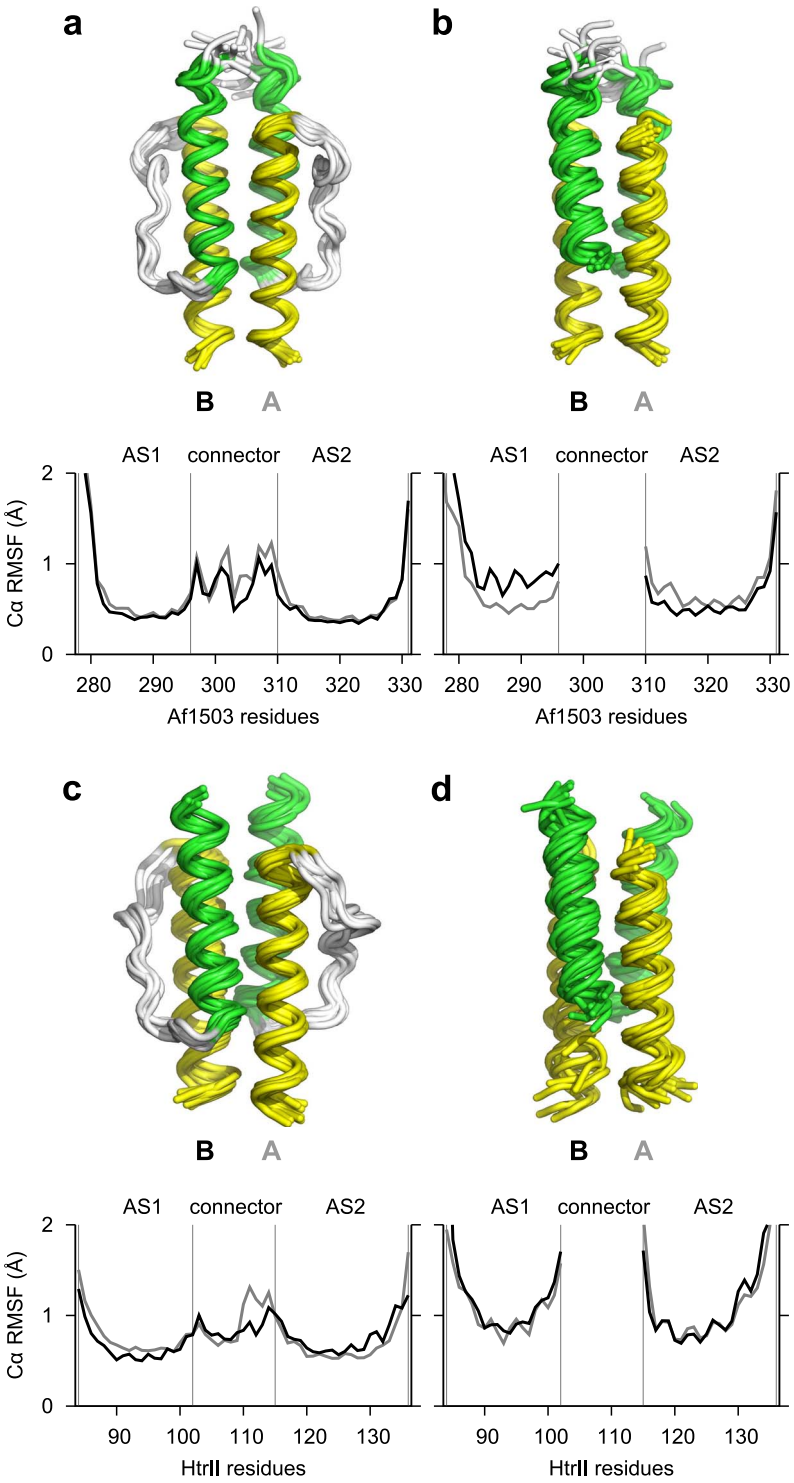

Figure 4 Superimposition of snapshots taken from the trajectory with 10 ns interval (a, b, d) or 20 ns interval (c) (AS1 (green), AS2 (yellow), and the connector loop (white)). Also shown is the residue profile of the root mean square fluctuation (RMSF = $\langle(\mathbf{r}_i - \langle\mathbf{r}_i\rangle)^2\rangle^{1/2}$ where $\mathbf{r}_i$ is the coordinates of atom i superimposed upon the average structure $\langle\mathbf{r}_i\rangle$) for C_α atoms calculated for the trajectory of the last 50 ns (chain A (gray) and chain B (black) according to the chain identifier in PDBid: 2asw). (a) Af1503, (b) the Af1503 loop deletion mutant, (c) HtrII, and (d) the HtrII loop deletion mutant.

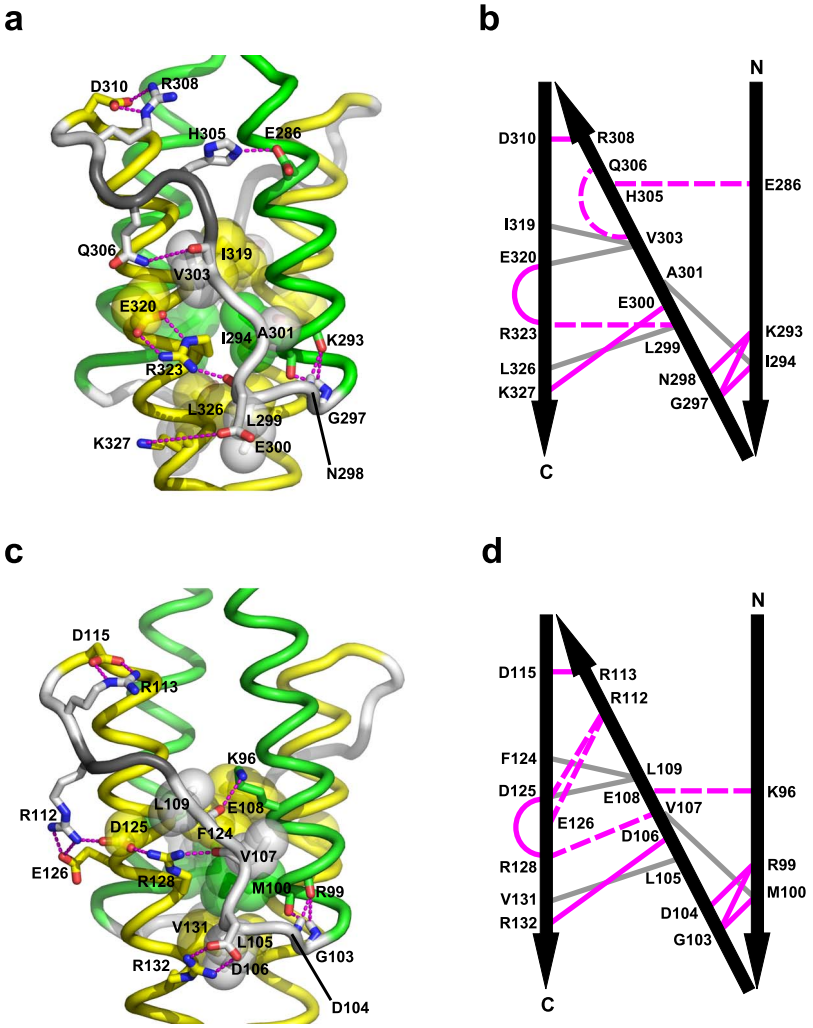

Figure 5 Polar and hydrophobic contacts involved in the HAMP domain connector loops. (a) A tube model of the Af1503 HAMP domain (taken from a snapshot of the trajectory at 100 ns). The color scheme of the chain is the same as that in Fig. 4, but the difference in the alignments of models 1 and 2 (residues 110–112; the gray shaded region in Fig. 1) is colored in dark gray. (b) Schematic representation of the contacts in Af1503. Magenta and gray lines represent polar and hydrophobic contacts, respectively. Solid lines indicate the contacts between the corresponding pairs of residues in Af1503 and HtrII. Broken lines represent contacts appearing in either of the two molecules. (c) Tube model of the HtrII HAMP domain (taken from a snapshot of the trajectory at 160 ns). (d) Schematic representation of the contacts in HtrII.

conserved hydrophobic contacts contribute to the stability of the connector loop, a conclusion supported by the HtrII homology model.

Contacts stabilizing the connector loop structure

Figures 5a and 5c compare polar and hydrophobic contacts in the HAMP domains of Af1503 and HtrII that are related to the stability of the connector loop. The interactions were defined according to LIGPLOT[31] with the default values of the criteria specified by HBPLUS[32]. The time courses of the interactions were summarized in Supplementary Fig. S2. As schematically shown in Figs. 5b and 5d, most of the contacts are conserved in both Af1503 and HtrII. Differences appear in the region containing the gap (304–307 in Af1503 and 110–112 in HtrII). The intra-loop interaction Q303-V306 in Af1503 was replaced by the inter-strand contacts R112-D125/E126 in HtrII. Interestingly, model 1 (Fig. 1) contacts more resembled those of Af1503 than model 2 (data not shown): an intra-loop contact L110-R112 (corresponding to V303-Q306 in Af1503) and an inter-strand contact L105-R128 (corresponding to L299-R323). However, since the loop in model 1 was not stable (Supplementary Fig. S1), we concluded that the set of the contacts in model 2, R112-D125/E126 and V107-R128, are important to maintain the stable structure of the connector loop in HtrII. The inter-chain interactions and a dynamic interaction in the C-terminal part of the AS1 are summarized in Supplementary Figs. S3 and S4.

Inter-helix packing: Coiled-coil structure

The inter-helical contacts in the coiled-coil structure serve as the main source of stability in the HAMP domains. The

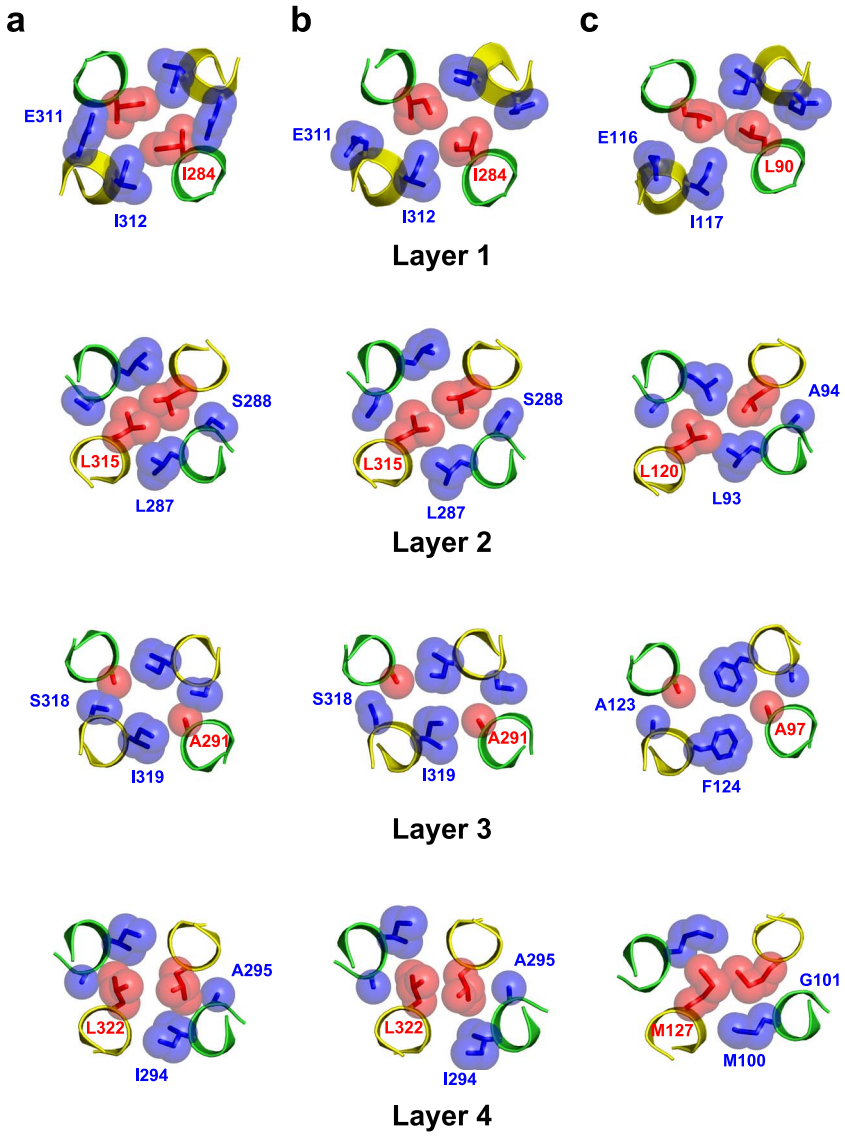

Figure 6 Cross sections of the four HAMP domain hydrophobic core layers (layer 1–layer 4), viewed from the N-terminal sides (from the top of the structures in Fig. 4). (a) NMR structure of Af1503 (PDBid: 2asw). (b) Simulated structure of Af1503 at 100 ns. (c) Simulated structure of HtrII at 100 ns. AS1 and AS2 helices are colored in green and yellow, respectively. The two helices at bottom represent chain A and those at top are chain B. The side-chain atoms of the *x*-positions are represented by red spheres, and those of the *da* positions by blue spheres. The knobs-into-holes packing form is achieved by rotations of the helices by +26° for AS1 (green) and −26° for AS2 (yellow).

coiled-coil packing in the NMR structure and the simulation results for Af1503 and HtrII are shown in Fig. 6. Hulko *et al.* argued that the Af1503 HAMP domain is characterized by unusual knobs-to-knobs (*x-da*) packing, which is related to canonical knobs-into-holes packing by a 26° rotation of each helix[12]. The NMR structure indicates that the side-chains of I284 and L315 at the *x*-position in layers 1 and 2, respectively, point toward the center of the coiled-coil (Fig. 6a). This is the characteristic form of knobs-to-knobs (*x-da*) packing. On the other hand, in the layer 4, L322 appears to be inserted into the pocket formed by I294 and A295 of the other chain. This feature is typical of knobs-into-holes (*a-d*) packing. Therefore, our data suggest that layers 1 and 2 exhibit *x-da* packing as argued by Hulko *et al.*[12], while layer 4 is clearly in the *a-d* packing state. However, the packing form cannot be rigorously determined by eye, particularly in the case of residues with small side-chains, such as A291 in layer 3. To overcome this limitation, we calculated the *side-chain crick angle* using TWISTER program[17].

Figure 7 shows the side-chain crick angles of the NMR structure and the simulation results, along with the average values of the GCN4 leucine zipper (PDBid: 1gcl[33]) as an example of typical knobs-into-holes packing of parallel four-helix coiled-coil (the calculated side-chain crick angles for GCN4 are given in Supplementary Fig. S5). Typical

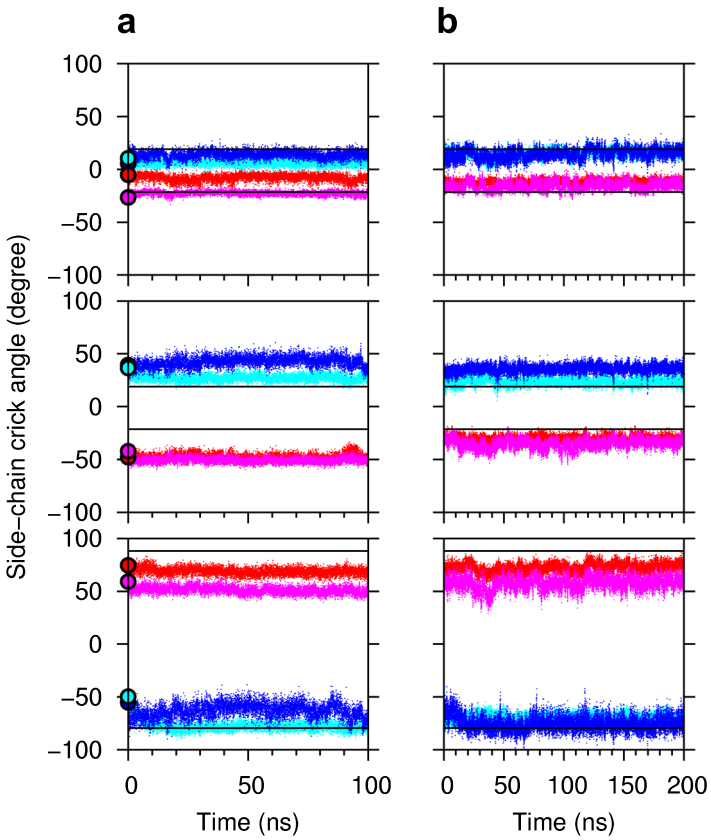

Figure 7 Side-chain crick angles of the residues located in the four hydrophobic core layers plotted against simulation time. (a) Af1503 and (b) HtrII. Top: *x*-positions; middle: *da*-positions in the intra-chain interactions; bottom: *da*-positions in the inter-chain interactions. Coloring scheme: Layer 1 (blue), Layer 2 (red), Layer 3 (cyan), and Layer 4 (magenta). The spheres at time 0 indicate the average angles of the NMR structure. As a reference, the side-chain crick angles of a typical knobs-into-holes packing of a parallel coiled-coil of GCN4 leucine zipper (PDBid: 1gcl[33]) are given by horizontal lines (top and middle: *a* at 19° and *d* at −21°; bottom: *e* at 88° and *g* at −79°). The calculated values for GCN4 leucine zipper are shown in Supplementary Fig. S5. A typical knobs-to-knobs packing of a parallel, coiled-coil may give 0° for *x*-position and ±52° for *da*-position. Detailed values are shown in Supplementary Tab. S1.

knobs-to-knobs packing in a parallel coiled-coil may yield 0° for the *x*-position and ±52° for the *da*-position. The side-chain crick angles were stable during the simulations, maintained to within about ±3°. A deviation of the magnitude is much smaller than the difference between the two sets of side-chain crick angles for knobs-to-knobs and knobs-into-holes packing. Assuming that the signal transduction hypothesis of Hulko *et al.*'s [12] is true, or assuming that the HAMP domain interconverts the coiled-coil structure between knobs-to-knobs and knobs-into-holes packing states upon signal reception, the side-chain crick angles would be expected to fluctuate to a greater extent between the knobs-to-knobs and knobs-into-holes forms even in the equilibrium state. The small amplitudes of rotational motion of the four helices observed in the simulations suggest that any transition between the two packing forms requires an external stimulation much larger than the thermal fluctuations.

Details regarding the calculation of the side-chain crick angles are shown in Supplementary Tab. S1. The average change of the side-chain crick angle indicates that in Af1503 the crick angle was maintained within 1° during the simulation. However, the crick angles data for HtrII reveals a clear tendency of shifting toward knobs-into-holes packing. Our results thus suggest that knobs-to-knobs packing is not common to all HAMP domains, and the type of packing form characteristic of the HAMP domain of a particular protein is determined by the amino acids involved in the inter-helical packing of the coiled-coil.

The key residues determining packing form in HtrII are F124 and M127 (corresponding to Af1503 residues I319 and L322, respectively). These amino acids significantly increase the bulkiness of the side-chains in the packing core region (Fig. 6). These amino acid changes cause an increase in the distance between the AS2 helix in chain A and the AS2 helix in chain B on which F124 and M127 are located. Concurrently, the intra-chain distance between AS1(chain A) and AS2(chain A) was largely increased (Fig. 8). However, the inter-chain distance between AS1(chain A) and AS2(chain B) was maintained, or even decreased. The side-chain packing in knobs-to-knobs is stabilized mainly by *x*-*x* contacts between AS1(chain A) and AS1(chain B) or

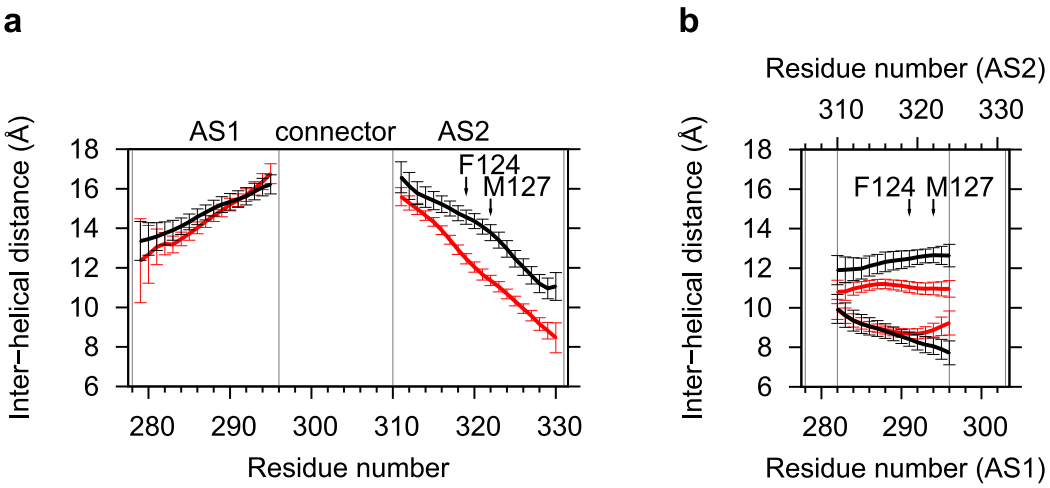

Figure 8 Inter-helical distances, defined by the distances between two helical axes, averaged for the last 50 ns of the simulations: Af1503 (red) and HtrII (black). The residue numbers shown are for Af1503 and are according to the alignment shown in Fig. 1. Vertical arrows indicate the locations of F124 and M127. Four different values of the average inter-helical distances are shown: (a) AS1(chain A)-AS1(chain B) and AS2(chain A)-AS2(chain B); (b) AS1(chain A)-AS2(chain A) (intra-chain; upper two curves) and AS1(A)-AS2(B) (inter-chain; lower two curves). In (b), the residue numbers are those of AS1.

between AS2(chain A) and AS2(chain B), and the intra-chain *x-da* contacts between AS1(chain A) and AS2(chain A). The side-chain packing in the knobs-into-holes form is stabilized primarily by inter-helical *a-d* contacts between AS1(chain A) and AS2(chain B). Therefore, we conclude that the changes in the distances associated with F124 and M127 (Fig. 6) destabilize the packing of the knobs-to-knobs form, and induce the knobs-into-holes packing form.

Note that in the SMART database of protein domains[34] we can find 46 halobacterial transducers, which contain 73 HAMP domains in total. Among them, 51 (70%) and 57 (78%) HAMP domains have Phe at the *a*-position in layer 3 and Met at the *d*-position in layer 4, respectively. This suggests that many halobacterial transducers may possess the similar structural feature as that in the HtrII HAMP domain, or knobs-into-holes packing.

Contributions of the connector loop to the HAMP domain stability

The many interactions that contribute to stabilizing the connector loop region of the HAMP domain were summarized in Fig. 5. We are interested in addressing the degree to which these interactions stabilize the coiled-coil structure, and to answer the question, we simulated the HAMP domain without the connector loops.

The results of the simulations are shown in Figs. 3 and 4. The RMSD values appeared to reach a plateau after 20–30 ns, and were increased only slightly above those in the simulations of Af1503 (0.30 Å, Fig. 3b) and HtrII (0.23 Å, Fig. 3d). The RMSF values for the simulations also showed small differences: deletion of the loops increased the RMSF value by 0.1 Å in Af1503 and 0.4 Å in HtrII, when excluding the terminal residues. Therefore, the HAMP domains can be maintained even without the connector loop, although deleting the connector loop does increase fluctuations. We conclude that the inter-helical packing at the interfaces of the coiled-coil structure is the primary source of the domain stability.

In conclusion, we have developed an atomic model of the HAMP domain of HtrII that is stable during the molecular dynamics simulation. The bulky side-chains characteristic of HtrII shift the packing state from an unusual knobs-to-knobs form as found in Af1503 to the canonical knobs-into-holes form. The connector loops do not play a critical role in maintaining structural stability. The model described here is being employed in molecular modeling of the sensory rhodopsin II/HtrII complex.

Acknowledgements

The simulations were performed at the Department of Supramolecular Biology, Yokohama City University, and at the Research Center for Computational Science, Okazaki, Japan. This work was supported by Grants-in-Aid for Scientific Research to AK from the Ministry of Education, Culture, Sports, Science, and Technology of Japan.

References

1. Hoff, W. D., Jung, K. H. & Spudich, J. L. Molecular mechanism of photosignaling by archaeal sensory rhodopsins. *Annu. Rev. Biophys. Biomol. Struct.* **26**, 223–258 (1997).
2. Falke, J. J., Bass, R. B., Butler, S. L., Chervitz, S. A. & Danielson, M. A. The two-component signaling pathway of bacterial chemotaxis: a molecular view of signal transduction by receptors, kinases, and adaptation enzymes. *Annu. Rev. Cell Dev. Biol.* **13**, 457–512 (1997).

3. Spudich, J. L. & Luecke, H. Sensory rhodopsin II: functional insights from structure. *Curr. Opin. Struct. Biol.* **12**, 540–546 (2002).
4. Sasaki, J. & Spudich, J. L. Signal transfer in haloarchaeal sensory rhodopsin-transducer complexes. *Photochem. Photobiol.* **84**, 863–868 (2008).
5. Moual, H. L. & Koshland, D. E., Jr. Molecular evolution of the C-terminal cytoplasmic domain of a superfamily of bacterial receptors involved in taxis. *J. Mol. Biol.* **261**, 568–585 (1996).
6. Rudolph, J., Nordmann, B., Storch, K. F., Gruenberg, H., Rodewald, K. & Oesterhelt, D. A family of halobacterial transducer proteins. *FEMS Microbiol. Lett.* **139**, 161–168 (1996).
7. Hazelbauer, G. L., Falke, J. J. & Parkinson, J. S. Bacterial chemoreceptors: high-performance signaling in networked arrays. *Trends Biochem. Sci.* **33**, 9–19 (2008).
8. Aravind, L. & Ponting, C. P. The cytoplasmic helical linker domain of receptor histidine kinase and methyl-accepting proteins is common to many prokaryotic signalling proteins. *FEMS Microbiol. Lett.* **176**, 111–116 (1999).
9. Williams, S. B. & Stewart, V. Functional similarities among two-component sensors and methyl-accepting chemotaxis proteins suggest a role for linker region amphipathic helices in transmembrane signal transduction. *Mol. Microbiol.* **33**, 1093–1102 (1999).
10. Gordeliy, V. I., Labahn, J., Moukhametzianov, R., Efremov, R., Granzin, J., Schlesinger, R., Büldt, G., Savopol, T., Scheidig, A. J., Klare, J. P. & Engelhard, M. Molecular basis of transmembrane signalling by sensory rhodopsin II-transducer complex. *Nature* **419**, 484–487 (2002).
11. Moukhametzianov, R., Klare, J. P., Efremov, R., Baeken, C., Göppner, A., Labahn, J., Engelhard, M., Büldt, G. & Gordeliy, V. I. Development of the signal in sensory rhodopsin and its transfer to the cognate transducer. *Nature* 440, 115–119 (2006).
12. Hulko, M., Berndt, F., Gruber, M., Linder, J. U., Truffault, V., Schultz, A., Martin, J., Schultz, J. E., Lupas, A. N. & Coles, M. The HAMP domain structure implies helix rotation in transmembrane signaling. *Cell* **126**, 929–940 (2006).
13. Swain, K. E. & Falke, J. J. Structure of the conserved HAMP domain in an intact, membrane-bound chemoreceptor: a disulfide mapping study. *Biochemistry* **46**, 13684–13695 (2007).
14. Zhou, Q., Ames, P. & Parkinson, J. S. Mutational analyses of HAMP helices suggest a dynamic bundle model of input-output signalling in chemoreceptors. *Mol. Microbiol.* **73**, 801–814 (2009).
15. Watts, K. J., Johnson, M. S. & Taylor, B. L. 2008. Structure-function relationships in the HAMP and proximal signaling domains of the aerotaxis receptor Aer. *J. Bacteriol.* **190**, 2118–2127 (2008).
16. Döbber, M., Bordignon, E., Klare, J. P., Holterhues, J., Martell, S., Mennes, N., Li, L., Engelhard, M. & Steinhoff, H. J. Salt-driven equilibrium between two conformations in the HAMP domain from *Natronomonas pharaonis*: the language of signal transfer? *J. Biol. Chem.* **283**, 28691–28701 (2008).
17. Strelkov, S. V. & Burkhard, P. Analysis of alpha-helical coiled coils with the program TWISTER reveals a structural mechanism for stutter compensation. *J. Struct. Biol.* **137**, 54–64 (2002).
18. Needleman, S. B. & Wunsch, C. D. A general method applicable to the search for similarities in the amino acid sequence of two proteins. *J. Mol. Biol.* **48**, 443–453 (1970).
19. Henikoff, S. & Henikoff, J. G. Amino acid substitution matrices from protein blocks. *Proc. Natl. Acad. Sci. USA* **89**, 10915–10919 (1992).
20. Dayhoff, M. O., Schwartz, R. M. & Orcutt, B. C. A model of evolutionary change in proteins. in *Atlas of Protein Sequence and Structure* (Dayhoff, M. O. ed) vol. 5, pp. 345–358 (National Biomedical Research Foundation, Washington, DC, 1979).
21. Sali, A. & Blundell., T. L. Comparative protein modelling by satisfaction of spatial restraints. *J. Mol. Biol.* **234**, 779–815 (1993).
22. Canutescu, A. A., Shelenkov, A. A. & Dunbrack, R. L., Jr. A graph theory algorithm for protein side-chain prediction. *Protein Science* **12**, 2001–2014 (2003).
23. Hooft, R. W. W., Vriend, G., Sander, C. & Abola, E. E. Errors in protein structures. *Nature* **381**, 272–272 (1996).
24. Laskowski, R. A., MacArthur, M. W., Moss, D. S. & Thornton, J. M. PROCHECK: a program to check the stereochemical quality of protein structures. *J. Appl. Cryst.* **26**, 283–291 (1993).
25. Ikeguchi, M. Partial rigid-body dynamics in NPT, NPAT and NPgammaT ensembles for proteins and membranes. *J. Comput. Chem.* **25**, 529–541 (2004).
26. Essmann, U., Perera, L., Berkowitz, M. L., Darden, T., Lee, H. & Pedersen, L. G. A smooth particle mesh Ewald method. *J. Chem. Phys.* **103**, 8577–8593 (1995).
27. MacKerell, A. D., Jr., Bashford, D., Bellott, R. L., Dunbrack, R. L., Jr., Evanseck, J. D., Field, M. J., Fischer, S., Gao, J., Guo, H., Ha, S., Joseph-McCarthy, D., Kuchnir, L., Kuczera, K., Lau, F. T. K., Mattos, C., Michnick, S., Ngo, T., Nguyen, D. T., Prodhom, B., Reiher III, W. E., Roux, B., Schlenkrich, M., Smith, J. C., Stote, R., Straub, J., Watanabe, M., Wiorkiewicz-Kuczera, J., Yin, D. & Karplus, M. All-atom empirical potential for molecular modeling and dynamics studies of proteins. *J. Phys. Chem. B.* **102**, 3586–3616 (1998).
28. Mackerell, A. D., Jr. Empirical force fields for biological macromolecules: overview and issues. *J. Comput. Chem.* **25**, 1584–1604 (2004).
29. Jorgensen, W. L., Chandrasekhar, J., Madura, J. D., Impey, R. W. & Klein, M. L. Comparison of simple potential functions for simulating liquid water. *J. Chem. Phys.* **79**, 926–935 (1983).
30. Ames, P., Zhou, Q. & Parkinson, J. S. Mutational analysis of the connector segment in the HAMP domain of Tsr, the Escherichia coli serine chemoreceptor. *J. Bacteriol.* **190**, 6676–6685 (2008).
31. Wallace, A. C., Laskowski, R. A. & Thornton., J. M. LIGPLOT: A program to generate schematic diagrams of protein-ligand interactions. *Protein Eng.* **8**, 127–134 (1995).
32. McDonald, I. K. & Thornton, J. M. Satisfying Hydrogen Bonding Potential in Proteins. *J. Mol. Biol.* **238**, 777–793 (1994).
33. Harbury, P. B., Zhang, T., Kim, P. S. & Alber, T. A switch between two-, three-, and four-stranded coiled coils in GCN4 leucine zipper mutants. *Science* **262**, 1401–1407 (1993).
34. Letunic, I., Doerks, T. & Bork, P. SMART 6: recent updates and new developments. *Nucleic Acids Res.* **37**, D229–232 (2009).